Raman Spectroscopy of Lithographically Patterned Graphene Nanoribbons

Sunmin Ryu,[†,*] Janina Maultzsch,[‡] Melinda Y. Han,[§,#] Philip Kim,[⊥] and Louis E. Brus[∥]

[†]Department of Applied Chemistry, Kyung Hee University, Yongin, Gyeonggi 446-701, Korea, [‡]Institut für Festkörperphysik, Technische Universität Berlin, 10623 Berlin, Germany, [§]Department of Applied Physics and Applied Mathematics, Columbia University, New York, New York 10027, United States, [⊥]Department of Physics, Columbia University, New York, New York 10027, United States, and [∥]Department of Chemistry, Columbia University, New York, New York 10027, United States. [#]Current affiliation: National Renewable Energy Laboratory, Golden, Colorado 80401, United States.

Graphene has attracted much interest as a novel two-dimensional material with great potential in future applications such as flexible and transparent electrodes,[1−3] electrical devices,[4] ultrathin membranes,[5] and various nanocomposites[6] due to its remarkable material properties. In particular, nanometer-sized graphene objects (NGOs) are becoming more highlighted in further manipulating the inherent properties of bulk graphene sheets. Graphene nanoribbons (GNRs) have early been predicted to behave as a semiconductor with a bandgap that is determined by ribbon width and chirality.[7] The dimension−bandgap correlation has been experimentally confirmed for lithographically patterned GNRs.[8] Field effect transistors (FETs) made of chemically derived GNRs of width <10 nm showed on−off current ratios of 10^7 at room temperature.[9] Under appropriate in-plane electric fields, zigzag-edged GNRs have been proposed to behave as a half-metal, which will be useful in spintronics on the nanometer scale.[10] As a networked nanostructure, graphene nanomeshes prepared by block copolymer lithography proved to carry 100 times larger current than individual GNR FETs[11] and also showed significant bandgaps.[12] Colloidal graphene quantum dots of variable size[13] and armchair-edged GNRs[14] were synthesized from molecular precursors and presented unique electronic and vibrational spectra, respectively.

Despite rising interest in quantum confinement effects of NGOs, optical characterization of their newly emerging properties has been rare.[13−16] In particular, Raman spectroscopy, widely used in characterizing bulk graphene sheets for their thickness,[17−19] structural integrity,[17,20−23] and charge density,[24,25] has not been systematically applied

ABSTRACT Nanometer-scale graphene objects are attracting much research interest because of newly emerging properties originating from quantum confinement effects. We present Raman spectroscopy studies of graphene nanoribbons (GNRs), which are known to have nonzero electronic bandgap. GNRs of width ranging from 15 to 100 nm have been prepared by e-beam lithographic patterning of mechanically exfoliated graphene followed by oxygen plasma etching. Raman spectra of narrow GNRs can be characterized by an upshifted G band and a prominent disorder-related D band originating from scattering at the ribbon edges. The D-to-G band intensity ratio generally increases with decreasing ribbon width. However, its decrease in width of <25 nm, partly attributed to amorphization at the edges, provides a valuable experimental estimate on D mode relaxation length of <5 nm. The upshift in the G band of the narrowest GNRs can be attributed to confinement effect or chemical doping by functional groups on the GNR edges. Notably, GNRs are much more susceptible to photothermal effects resulting in reversible hole doping caused by atmospheric oxygen than bulk graphene sheets. Finally we show that the 2D band is still a reliable marker in determining the number of layers of GNRs despite its significant broadening for very narrow GNRs.

KEYWORDS: graphene nanoribbons · Raman spectroscopy · chemical doping · defects · phonon confinement effects

to NGOs, presumably due to insufficient Raman sensitivity.[8] As more NGOs are being studied, however, it has become ever important to have reliable tools to analyze their properties. It is not clear whether the 2D band[17−19] can still be used in differentiating single (1 L) from double (2 L) or multilayered (n L) NGOs. Because of the increased fraction of edge carbons in NGOs, the disorder-related D band intensity may not be useful in accessing their degree of structural defects. Functional groups at edges may further affect NGOs' electronic structures,[15,26] in particular, the Fermi level, by inducing extra charges,[27] which can be readily monitored by the positions of the G and 2D bands.[24,25] Since theory predicts that degeneracy between transverse and longitudinal G bands of GNRs is to be lifted due to confinement,[28] it is of immediate importance to verify the size effect on their lattice vibrations.[28−31]

Figure 2. Raman spectra of GNR sets *a, b, c, d, g* (see Figure 1) taken for sample I as prepared without further treatment. Excited with laser wavelength λ = 632.8 nm. The spectra were offset for clarity. The bands at 1450 and 1650 cm^{-1} are due to underlying Si and a plasma line of the excitation laser, respectively.
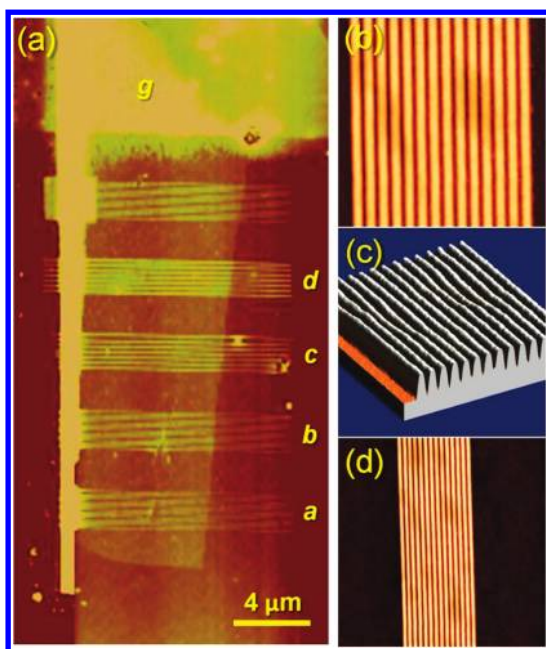
Figure 1. (a) AFM height image of sample I with GNR sets of varying width (*a*: 15 nm, *b*: 25 nm, *c*: 50 nm, *d*: 100 nm, *g*: bulk graphene). The image was taken after patterning 40 nm thick ribbon masks of HSQ and before removing unmasked graphene by oxygen plasma. Instrumental interference during AFM imaging caused Moiré patterns along the GNRs, which blurred the observed topography. (b) AFM height image ($2.5 \times 2.5 \ \mu m^2$) of 50 nm wide GNRs in sample II. (c) Three-dimensional representation of the image in (b). (d) AFM height image ($6 \times 6 \ \mu m^2$) of 50 nm wide GNRs in sample II.

Here we present systematic Raman spectroscopy studies of lithographically patterned GNRs. The nominal width (w_{nom}) ranges from 15 to 100 nm. While the relative intensity of the D band generally increases with decreasing width, it starts to decrease for the narrowest GNRs due to the increasing fraction of disordered areas at the edges. We also observe an upshift in the G band and drastic broadening in the G and 2D bands for the narrowest GNRs, which can be attributed to the size and edge effects. GNRs were also found to be much more sensitive to photothermally induced hole doping than bulk graphene sheets, which stresses that additional caution is required in diagnostic use of Raman spectroscopy for NGOs.

RESULTS AND DISCUSSION

The GNRs were prepared by lithographic patterning of hydrogen silsesquioxane (HSQ), a negative-tone resist, into protective etch masks followed by O_2 plasma etching of the unprotected graphene area (see Methods).[8] Figure 1 shows AFM height images of sample I and sample II taken before (Figure 1a) and after (Figure 1b, c, and d) O_2 plasma etching, respectively. The nominal widths of the GNRs were 15, 25, 50, and 100 nm for sample I and 15, 50, and 100 nm for sample II. Figure 2 presents the Raman spectra of GNRs as prepared (sample I). The spectra show the G band derived from the zone-center optical E_{2g} phonon in graphene and
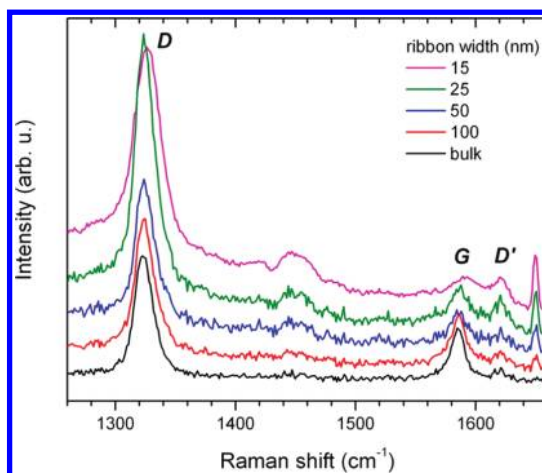
two defect-induced bands denoted D and D′. Although the peak positions and intensities vary slightly from spot to spot, the overall spectral features were well reproduced within an array. The G band energy is virtually the same between the bulk patch and GNRs of width down to 25 nm. For the narrowest GNRs (15 nm), however, the G band upshifts by ~5 cm^{-1} and broadens significantly. In addition, the G band was found to upshift further during repeated measurements, which suggests photoinduced effects that will be discussed later.

The two defect-induced bands at ~1330 cm^{-1} (D band) and ~1620 cm^{-1} (D′ band) dominate the spectra as the ribbon width decreases. Figure 3 shows the integrated intensity ratio of the D band to G band (I_D/I_G) as a function of the ribbon width. As the width decreases, the I_D/I_G increases significantly for both 1 L and 2 L GNRs. The increasing D band intensity is due to the increasing fraction of edge carbons, which serve as defects by breaking the translational symmetry of the lattice.[17,23] Since the employed e-beam lithography process is known to hydrogenate the basal plane forming C−H defects,[21] the I_D/I_G ratio was also measured following two cycles of thermal dehydrogenation at 100 and 200 °C.[32] The annealing decreases the I_D/I_G of the bulk graphene patch from 3.4 to 0.52; however, it barely affects that of narrow GNRs (width ≤50 nm), indicating that their basal plane C−H defects contribute much less than the ribbon edges in activating the D band (see Figures S1 and S2 for Raman spectra of dehydrogenated GNRs). The 2 L GNRs also show a similar increase in the I_D/I_G ratio with decreasing ribbon width. Note that the patterning-induced basal plane hydrogenation is negligible in 2 L graphene, as was shown by zero I_D/I_G ratio for the bulk.[21]
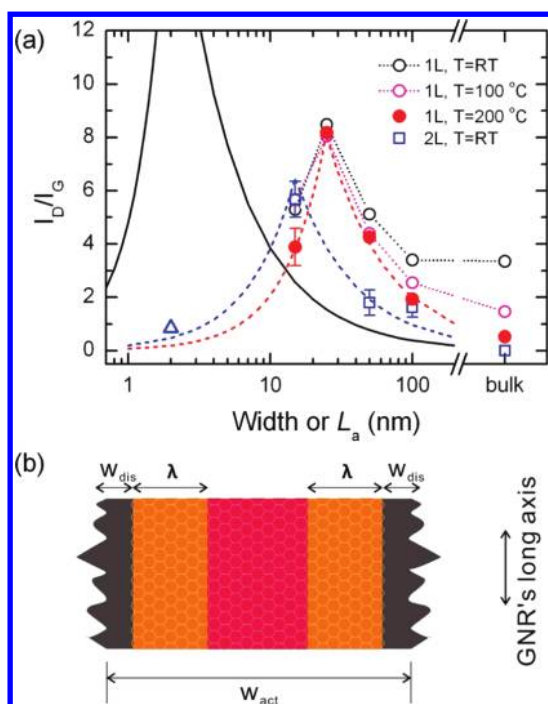
Figure 3. (a) Integrated intensity ratio (I_D/I_G) of the D band to the G band as a function of the ribbon width (w_{nom}): 1 L (circle, sample I) and 2 L (square, sample II) GNRs; black circles were obtained from GNRs as prepared, magenta circles from GNRs annealed at 100 °C, red solid circles from GNRs annealed at 200 °C; blue squares from GNRs as prepared; open triangle is for 2 nm wide 2 L GNR from ref 36. Solid lines represent the empirical relations: $I_D/I_G \approx L_a^{-1}$ for $L_a > 2$ nm (refs 33, 34) and $I_D/I_G \approx L_a^2$ for $L_a < 2$ nm (ref 23). They were calculated based on refs 23 and 34 using continuity at $L_a = 2$ nm (ref 23). Dashed and dotted lines are to guide the eye. (b) Schematic model of lithographically patterned GNR of $w_{act} = w_{nom} - 10$ nm. λ and w_{dis} are the relaxation length of the D band and width of disordered regions at edges, respectively.

For polycrystalline graphite, the I_D/I_G ratio correlates with effective domain size: with decreasing crystallite size (L_a), the ratio increases as L_a^{-1} for $L_a > 2$ nm[33,34] and decreases as L_a^2 below ~2 nm (solid lines in Figure 3a).[23,35] The decrease for $L_a < 2$ nm was attributed to increasing fraction of amorphous sp^2 carbons, which contribute to the G band but not the D band.[23,35] We find that GNRs also show a similar scaling behavior: with decreasing width, the I_D/I_G of 1 L GNRs increases, reaching a maximum at w_{nom} of 25 nm, and then decreases for the narrower GNRs ($w_{nom} = 15$ nm). While 2 L GNRs obey a similar rule, their I_D/I_G ratios are smaller than those of 1 L ones. If Wang et al.'s Raman measurement for ~2 nm wide GNR[36] is included, it is clear that 2 L GNRs also have a maximum I_D/I_G ratio at width ≤15 nm.

The observed change in the scaling laws at a width of 15−25 nm provides an experimental confirmation of length scale for the Raman scattering process of the D band.[37,38] In the double-resonance process for the D mode phonon, an electron−hole pair generated by Raman excitation laser will propagate a certain distance, λ, during their lifetime, which is limited by the uncertainty
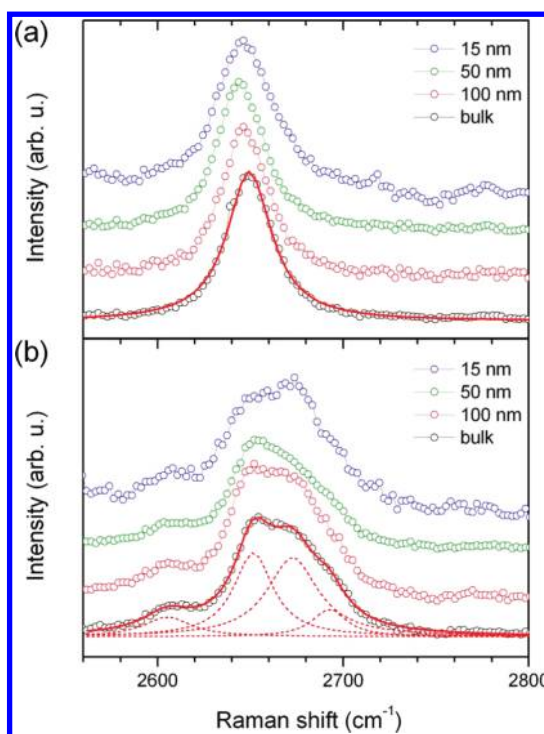

Figure 4. 2D band Raman spectra of GNRs and bulk graphene sheets annealed in Ar at 100 °C for 1 h: (a) 1 L and (b) 2 L (sample II). Red solid and dotted lines for bulk graphene sheets represent Lorentzian fits ($\lambda_{excitation} = 632.8$ nm).

principle.[37,39] Since the electron needs to be scattered off a defect to satisfy the momentum conservation rule,[40] the origin of the electron−hole pair needs to be within λ from defects for the D band to be observed. The actual width (w_{GNR}) of GNRs prepared by identical methods is typically ~10 nm smaller than the nominal width due to overetching underneath the HSQ etch mask.[8] The narrowest GNRs of $w_{nom} = 15$ nm employed in the current study are likely ~5 nm wide. The extent of overetching, however, should depend on various processing parameters. In addition, narrow areas (<2 nm, dark area of w_{dis} in width in Figure 3b) of the GNR edges are thought to be highly disordered due to O_2 plasma etching.[8,41] While the G band can be observed from such strongly disordered sp^2 carbon networks, the D band cannot, due to the lack of 6-fold rings.[23,35] For a model GNR schematically shown in Figure 3b, the central area (shown in red) located beyond $w_{dis} + \lambda$ from either edge does not contribute to the D band while still giving the G band signal. This reasoning leads to a conclusion that a maximum I_D/I_G ratio will be obtained for a GNR of $w_{GNR} = 2\lambda + 2w_{dis}$. Given that $w_{nom} = 15−25$ nm for a maximum I_D/I_G ratio in Figure 3a and $w_{nom} = w_{GNR} + 10$ nm, we find that λ is in the range 1−5 nm, which is consistent with ~4 nm deduced from an argument based on lifetime and velocity of electrons.[37] Our result is also in good agreement with the Raman relaxation length (2 nm) determined for ion-bombarded bulk graphene sheets by Raman spectroscopy combined with STM.[38]
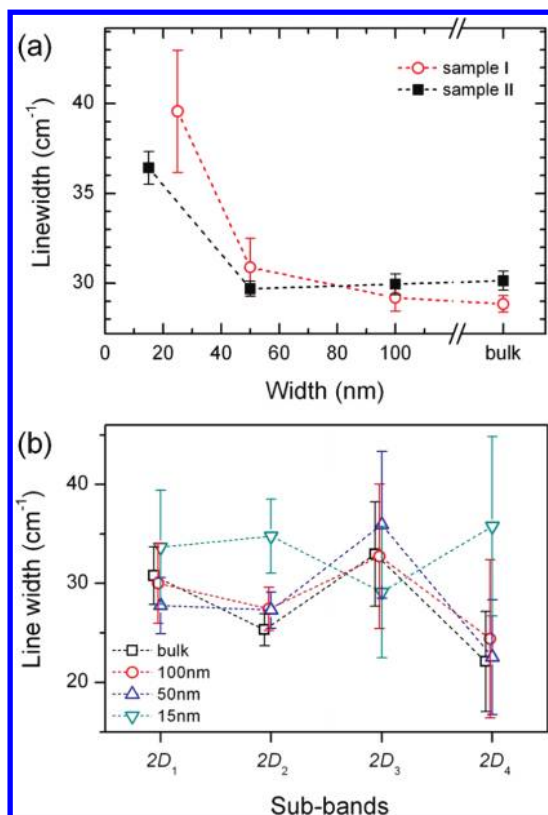
Figure 5. (a) Line width of the 2D band of 1 L GNRs as a function of ribbon width (w_{nom}). (b) Line width of the 2D band of 2 L GNRs decomposed into four sub-bands.
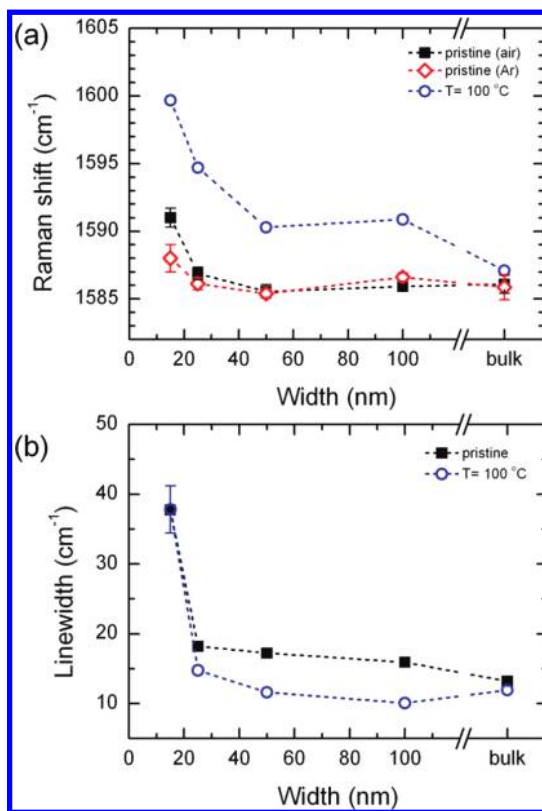

Figure 6. G band energy (a) and line width (b) of 1 L GNRs as a function of ribbon width: (squares) as prepared, (circles) after annealing at 100 °C. Diamonds in (a) were taken for the as-prepared sample under an Ar atmosphere instead of in air. The data were obtained from Figure 2 and Figure S1.

It is also notable that 1 L GNRs give I_D/I_G ratios much larger than 2 L ones of the same width (w_{nom}) and graphite crystallites of $L_a = w_{nom}$: more appropriate graphene analogues for graphite crystallites of domain size L_a will be graphene nanodisks of diameter L_a. However, the nanodisks will give higher I_D/I_G than GNRs of width L_a because of the former's larger fraction of edge carbons. This implies that NGOs obey the above empirical relationships[23,33] qualitatively, but the detailed relation is thickness-dependent. It is also to be noted that I_D/I_G ratios of GNRs should depend on the polarization direction of the incoming and scattered light due to the one-dimensional nature of the GNRs[42] and polarization sensitivity of D band scattering off the graphene edge.[37]

Raman scattering has been one of the most efficient and nondestructive tools to determine thickness of graphene samples.[17−19] Thus, it is an interesting question whether or not the optical diagnosis is still valid for NGOs. Figure 4a shows 2D band Raman spectra of 1 L GNRs as well as 1 L bulk graphene. The 2D band of the GNRs can be well described with a single Lorentzian function, and GNRs of $w_{nom} \geq 50$ nm are not distinguishable from the bulk graphene in terms of the 2D band's line width (30 ± 1 cm^{-1}). As can be seen in Figure 5a, however, the 2D bands of sub-25 nm GNRs are noticeably broader than those of the rest. For 2 L GNRs shown in Figure 4b, the four sub-bands[17] of the

2D band persist even in the narrowest GNRs. However, the narrowest GNRs can be distinguished from the rest: (i) their peak frequency difference between the two central sub-bands is 4 cm^{-1} larger than that of the rest (21 ± 1 cm^{-1}); (ii) their sub-bands, except for 2D$_3$, are 5−10 cm^{-1} broader than those of the wider GNRs. The broadening of the 2D bands (Figure 5) and the G band (Figure 2 and Figure 6b) can be attributed to relaxation of the momentum conservation rule in finite-size domains[23] and heterogeneity near GNR edges, as will be discussed below. Despite the broadening, it is clear that Raman spectroscopy can be utilized in determining the number of layers in GNRs and possibly other NGOs as small as ∼5 nm in lateral dimension.

Besides the broadening, the G band of the narrowest GNRs in Figure 2 has ∼5 cm^{-1} higher frequency than wider ones (also see solid squares in Figure 6a). Interestingly, we found that the unusually high G band frequency of the narrowest GNRs is partly due to oxygen in the air and can be partially reversed in an inert atmosphere: the G band downshifts by ∼3 cm^{-1} when measured in Ar gas (open diamonds in Figure 6a). This indicates that the stiffening of the G band is largely caused by reversible binding of oxygen on GNRs. A similar sensitivity toward oxygen has been observed for thermally annealed graphene and pristine graphene

with high G band frequency.[43] However, we also note that the G band frequency of the narrowest GNRs is still a few cm^{-1} higher than wider GNRs even in inert Ar atmosphere, which may be attributed to a quantum confinement effect in GNRs.[28−31] Theory predicts that new boundary conditions in GNRs lift the degeneracy of the E_{2g} G mode.[28] With decreasing the width of GNRs, the transverse G mode subject to confinement across the GNRs blue-shifts several times more than the longitudinal mode. The frequency splitting between the two orthogonal modes, pseudolinearly decreasing with increasing width, amounts to 10−30 cm^{-1} for GNRs of 2.5 nm.[31] Since the narrowest GNRs in the current study are thought to have a width of ∼5 nm, a non-negligible confinement effect can be expected. More specifically, the unusually high G frequency and large line width of G and 2D bands found for the narrowest GNRs can be attributed to the size effects.

Alternatively, functional groups at ribbon edges may be responsible for the anomalies in the narrow GNRs. As the ribbon width decreases, the edges represent a larger fraction of total carbons and thus become more important. In particular, our ribbons were patterned using oxygen plasma, a harsh oxidizing condition, which is known to form various oxygen-containing functional groups on graphite.[44] Since oxygen is more electronegative than carbon, such functional groups are expected to withdraw π electrons of GNRs (i.e., dope with holes). Partially oxidized graphene sheets indeed show a significant upshift of the G mode frequency.[20] Given the observed ∼2 cm^{-1} difference between the narrowest GNRs and the rest is due to edge functional groups, an average charge density difference of ∼2 × 10^{12} cm^{-2} can be estimated on the basis of the electrical gating measurements.[24,25] While we do not know the exact chemical identities and density of functional groups on the edges, we can estimate how much charge is transferred by one functional group with simple geometric considerations. Since an ideal armchair (zigzag) edge has 4700 (4000) edge carbons/μm, the edge carbon density of 15 nm wide GNRs is 6.2 × 10^{13} (5.3 × 10^{13}) cm^{-2}. For this model GNR, ∼0.03 charges would be required per edge carbon attached to one oxygen-containing functional group, which is not unrealistic.[45,46] However, edges of lithographically patterned nanoribbons are very rough and contain highly disordered regions.[8] Moreover, charge density induced by edge functional groups should vary from the edges to the center of the GNRs. The unusually broad G band of the narrowest GNRs can be attributed to such geometric imperfection and charge inhomogeneity.

In the presence of oxygen, further stiffening of the G band is induced by prolonged irradiation of the Raman excitation laser, as can be seen in the progressive stiffening of the 25 nm wide GNRs (Figure 7a). The photoinduced stiffening in Ar gas, however, is several
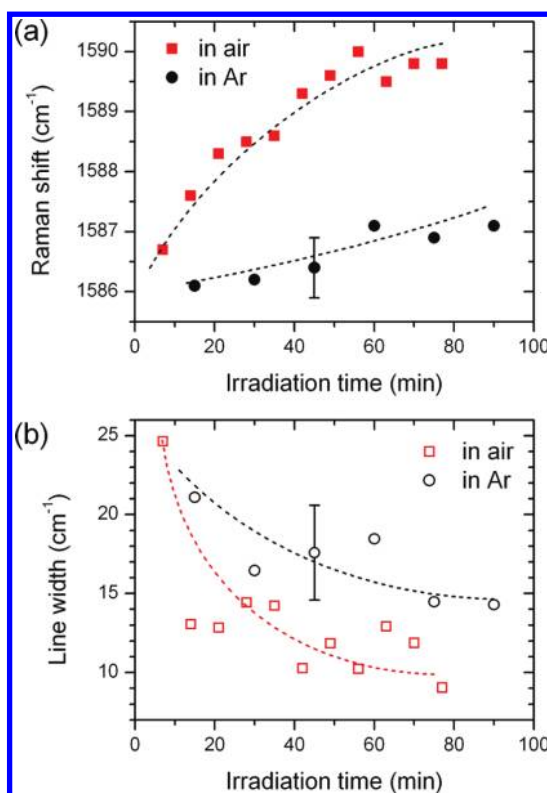

Figure 7. Changes in the G band (a) frequency and (b) line width of 1 L 25 nm wide ribbons (sample I, as prepared) caused by photoirradiation at 633 nm: (squares) in air, (circles) under an Ar atmosphere. The power density on the irradiated area (diameter ∼1.5 μm) was 300 kW/cm^2. Dotted line is to guide the eye.

times less, which may be attributed to impurity-level residual oxygen in the Ar gas or other unknown origins. The narrowing of the G band (Figure 7b) concurrent with the stiffening indicates that the changes can be explained by the charge doping theory:[24,25] as the Fermi level is displaced from its neutrality point by charge doping, nonadiabatic electron−phonon coupling causes the G band to stiffen. Simultaneously, the line width of the G band decreases since Landau damping of the G phonon is not allowed when the Fermi level is located more than half of the G band energy away from the neutrality point.

The photoinduced changes in the G band are similar to what was observed in thermally annealed bulk graphene sheets.[20,21,43,47−50] To see the effect of thermal annealing on GNRs, the sample in Figure 6 was reinvestigated following annealing at 100 °C in the air. It is notable that the G band frequency increased by 5−8 cm^{-1} for the GNRs, while it remained within 1 cm^{-1} for the bulk patch (blue circles in Figure 6a). At the same time, the G band line width of the ribbons except the narrowest one decreased by 4−6 cm^{-1} (Figure 6b), which confirmed that the change is mostly driven by charge doping process. Stiffening of the D band (Figure S3), thus the 2D band, concurrent with that of the G band indicates that doped charges are
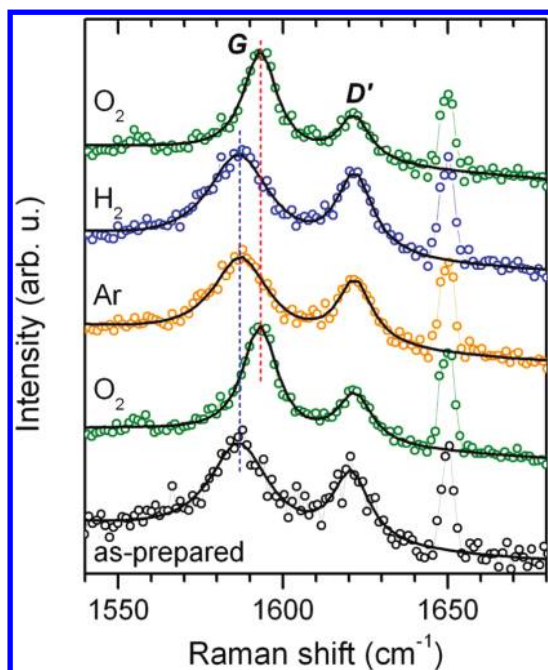
Figure 8. Raman spectra of 25 nm wide ribbons (sample I) obtained in various ambient gases. The bottom spectrum was taken in O_2 for as-prepared ribbons, and the four remaining spectra were taken after annealing at 100 °C for 2 h. The spectra are offset for clarity. Circles are experimental data, and solid lines represent double Lorentzian fits with linear backgrounds. The plasma lines at ~1650 cm^{-1} originating from the excitation laser were excluded from the fitting.

mainly holes.[51] However, there was no significant change in the line width of the D band (Figure S3).

The gas sensitivity of the G band and D band can be seen respectively in Figure 8 and Figure S4, where the Raman spectra of 25 nm wide GNRs were obtained in various gas environments before and after 100 °C annealing. We found that the stiffening and narrowing of the G band and stiffening of the D band correlate specifically with oxygen but not with other gases. The O_2-induced upshifts of 6 and 2 cm^{-1} respectively for the G and D bands are reversible (also see Figure S5). We also found that oxygen stiffens the 2D band as well as the G and D bands (Figure S6). There was no noticeable difference between measurements in pure oxygen and air. On the basis of the identical sensitivity toward oxygen leading to the stiffening and narrowing of the G band, we conclude that the photoinduced effects are mainly caused by photothermal annealing of the GNRs.

It is interesting to note that thermally induced blueshifts in the G band frequency are significantly larger for GNRs than bulk graphene sheets (Figure 6). Ryu *et al.* showed that the annealing-induced hole doping in bulk graphene sheets is directly caused by oxygen (O_2) and that the sensitivity to oxygen is greatly enhanced by thermally induced formation of nanometer-sized ripples.[43] Annealing can make graphene conform better to atomically rough SiO_2 substrate by driving out extraneous impurities trapped in the gap, which can
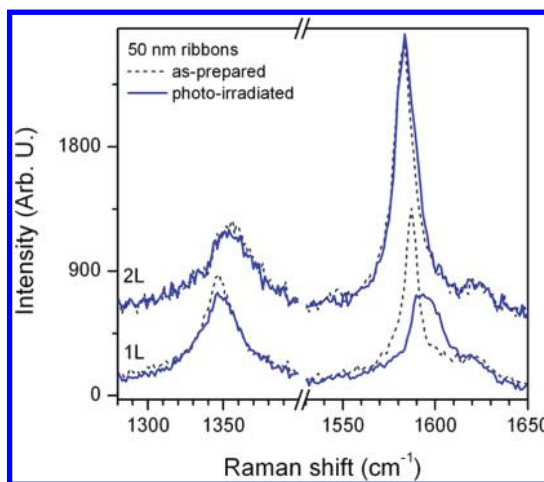

Figure 9. G band Raman spectra of 1 L and 2 L 50 nm wide ribbons (sample II, as prepared) taken (dotted) before and (solid) after 10 min photoirradiation at 514 nm. The power density on the irradiated area (diameter ~1 μm) was 300 kW/cm^2.

lead to enhanced corrugation in graphene.[43] In an alternative explanation, heating causes graphene with a negative thermal expansion coefficient (TEC) to shrink and slide against the expanding SiO_2 substrate with positive TEC,[52] and the opposite differential expansion during cooling cycles can cause graphene to buckle in the out-of-plane direction, forming ripples.[43] In GNRs, the thermal rippling can be readily explained by either of the two models: In the former, molecular species trapped underneath the GNRs can diffuse out very efficiently at elevated temperature due to their small width. In the latter, the total adhesive force between the GNRs and substrate, which resists sliding during heating, will be proportionally small for narrow GNRs.

The photoinduced effect is also dependent on the thickness of the GNRs. Figure 9 shows Raman spectra taken in the air for 1 L and 2 L 50 nm wide GNRs before and after prolonged photoirradiation of the 514 nm Raman excitation laser. Upon irradiation, the G band of 1 L GNRs is upshifted by 7 cm^{-1}, while that of 2 L GNRs remained unchanged. This directly shows that the photothermal effect is much larger in 1 L than 2 L GNRs. Since thicker graphene sheets are stiffer,[53] formation of ripples requiring graphene sheets to deform in the out-of-plane direction should be less favored with increasing thickness. Similar thickness dependences of chemical activity have been observed in thermal oxidation,[20] hydrogenation,[21] photochemical,[22] and electron transfer reactions[54] of bulk graphene sheets. We also note that the photoirradiation in Figure 9 caused no significant structural defects. In fact, the D band intensity decreased following the irradiation, indicating that the observed changes in the G band are not associated with formation of defects. The decrease in the D band intensity is due to the aforementioned photothermal removal of hydrogen atom defects bound to the basal plane of the

GNRs.[21] Dehydrogenation itself was found to affect the G band frequency negligibly.[21]

CONCLUSIONS

In summary, we presented Raman spectroscopy studies for lithographically patterned GNRs of widths ranging from 15 to 100 nm. Despite significant broadening for narrow GNRs, the 2D band can still be used in determining the number of layers even for $w_{GNR} \approx$ 5 nm (w_{nom} = 15 nm). The Raman spectra of 1 L GNRs are characterized by an upshift of the G band frequency and by an increase of the I_D/I_G ratio with decreasing width. The decrease in the I_D/I_G ratio for the narrowest GNRs is attributed to amorphization near ribbon edges. The narrowest GNRs as prepared show significant broadening in both G and 2D bands and non-negligible blue-shifts in the G band, which can be attributed to the confinement effect and/or chemical doping from oxygen-containing groups at the GNR edges. Reversible chemical doping is considerably enhanced by laser irradiation in the presence of oxygen, which is attributed to structural deformation caused by photothermal annealing. The 2 L GNRs, however, show immunity toward photoinduced effects. Spectroscopic features of GNRs revealed in the current studies should contribute to characterization and application of various graphene nanostructures.

METHODS

The GNRs were prepared by lithographic patterning followed by oxidative etching.[8] The 1 L and 2 L graphene sheets were deposited onto Si substrates with a 300 nm thick SiO$_2$ layer by mechanical exfoliation of Kish graphite. then 40 nm thick hydrogen silsesquioxane (HSQ), a negative-tone resist, was spin-coated onto the substrate. Following e-beam lithographic patterning of GNRs and subsequent development of the etch mask pattern, the unmasked graphene area was etched by O$_2$ plasma. Since the HSQ overlayers are difficult to remove[8] and do not interfere with the optical measurements,[21] all the measurements were conducted with the GNRs capped by the HSQ layers. In sample I made of 1 L graphene (Figure 1), the nominal GNR widths in the four arrays under study were 15, 25, 50, and 100 nm; their length was 8−10 μm. To increase the Raman signal, 6−10 GNRs of the same width were patterned in each array spanning 2 μm. Neighboring arrays were separated by 2 μm. All GNRs were oriented along the same direction. One large graphene patch (∼8 μm across) served as a reference bulk graphene. Sample II, with 1 L and 2 L GNRs, was prepared similarly (Figure 1). Raman measurements were performed with a home-built micro-Raman setup in backscattering geometry, using a He−Ne laser and an Ar ion laser for 633 and 514 nm excitations, respectively. The apparent diameters of focal spots were ∼1.5 μm for 633 nm and ∼1 μm for 514 nm. The spectral resolution limited by the overall instrumental response was 3.7 cm^{-1} for 633 nm and 2.2 cm^{-1} for 514 nm. While the polarization of the incoming light was parallel to the long axis of the GNRs, the scattered light was guided to a detector without further selection of polarization. All the measurements were done in ambient conditions except experiments where samples were placed in an environment-controlled optical cell. The pressure inside the cell was slightly above the atmospheric pressure, and the typical gas flow rate was 0.20 L/min.

Supporting Information Available: Raman spectra of GNRs annealed at 100 and 200 °C, analysis of D band of GNRs of varying width, gas sensitivity of D band of 25 nm wide GNRs, analysis of G band of 25 nm wide GNRs in response to various gases, O$_2$ sensitivity of 2D Raman bands of 25 nm wide GNRs.

This material is available free of charge *via* the Internet at http://pubs.acs.org.

REFERENCES AND NOTES

1. Eda, G.; Fanchini, G.; Chhowalla, M. Large-Area Ultrathin Films of Reduced Graphene Oxide as a Transparent and Flexible Electronic Material. *Nat. Nanotechnol.* **2008,** *3,* 270.
2. Kim, K. S.; Zhao, Y.; Jang, H.; Lee, S. Y.; Kim, J. M.; Kim, K. S.; Ahn, J.-H.; Kim, P.; Choi, J.-Y.; Hong, B. H. Large-Scale Pattern Growth of Graphene Films for Stretchable Transparent Electrodes. *Nature* **2009,** *457,* 706–710.
3. Bae, S.; Kim, H.; Lee, Y.; Xu, X. F.; Park, J. S.; Zheng, Y.; Balakrishnan, J.; Lei, T.; Kim, H. R.; Song, Y. I.; *et al.* Roll-to-Roll Production of 30-Inch Graphene Films for Transparent Electrodes. *Nat. Nanotechnol.* **2010,** *5,* 574–578.
4. Geim, A. K.; Novoselov, K. S. The Rise of Graphene. *Nat. Mater.* **2007,** *6,* 183–191.
5. Bunch, J. S.; Verbridge, S. S.; Alden, J. S.; Zande, A. M. v. d.; Parpia, J. M.; Craighead, H. G.; McEuen, P. L. Impermeable Atomic Membranes from Graphene Sheets. *Nano Lett.* **2008,** *8,* 2458–2462.
6. Wakabayashi, K.; Pierre, C.; Dikin, D. A.; Ruoff, R. S.; Ramanathan, T.; Brinson, L. C.; Torkelson, J. M. Polymer-Graphite Nanocomposites: Effective Dispersion and Major Property Enhancement Via Solid-State Shear Pulverization. *Macromolecules* **2008,** *41,* 1905–1908.
7. Son, Y.-W.; Cohen, M. L.; Louie, S. G. Energy Gaps in Graphene Nanoribbons. *Phys. Rev. Lett.* **2006,** *97,* 216803/1–216803/4.
8. Han, M. Y.; Oezyilmaz, B.; Zhang, Y.; Kim, P. Energy Band-Gap Engineering of Graphene Nanoribbons. *Phys. Rev. Lett.* **2007,** *98,* 206805/1–206805/4.
9. Li, X. L.; Wang, X. R.; Zhang, L.; Lee, S. W.; Dai, H. J. Chemically Derived, Ultrasmooth Graphene Nanoribbon Semiconductors. *Science* **2008,** *319,* 1229–1232.
10. Son, Y.-W.; Cohen Marvin, L.; Louie Steven, G. Half-Metallic Graphene Nanoribbons. *Nature* **2006,** *444,* 347–9.
11. Bai, J. W.; Zhong, X.; Jiang, S.; Huang, Y.; Duan, X. F. Graphene Nanomesh. *Nat. Nanotechnol.* **2010,** *5,* 190–194.
12. Liang, X. G.; Jung, Y. S.; Wu, S. W.; Ismach, A.; Olynick, D. L.; Cabrini, S.; Bokor, J. Formation of Bandgap and Subbands in Graphene Nanomeshes with Sub-10 nm Ribbon Width Fabricated Via Nanoimprint Lithography. *Nano Lett.* **2010,** *10,* 2454–2460.
13. Yan, X.; Cui, X.; Li, B. S.; Li, L. S. Large, Solution-Processable Graphene Quantum Dots as Light Absorbers for Photovoltaics. *Nano Lett.* **2010,** *10,* 1869–1873.
14. Cai, J. M.; Ruffieux, P.; Jaafar, R.; Bieri, M.; Braun, T.; Blankenburg, S.; Muoth, M.; Seitsonen, A. P.; Saleh, M.; Feng, X. L.; *et al.* Atomically Precise Bottom-up Fabrication of Graphene Nanoribbons. *Nature* **2010,** *466,* 470–473.

15. Barone, V.; Hod, O.; Scuseria, G. E. Electronic Structure and Stability of Semiconducting Graphene Nanoribbons. *Nano Lett.* **2006,** *6,* 2748–2754.

16. Jiao, L. Y.; Zhang, L.; Wang, X. R.; Diankov, G.; Dai, H. J. Narrow Graphene Nanoribbons from Carbon Nanotubes. *Nature* **2009,** *458,* 877–880.

17. Ferrari, A. C.; Meyer, J. C.; Scardaci, V.; Casiraghi, C.; Lazzeri, M.; Mauri, F.; Piscanec, S.; Jiang, D.; Novoselov, K. S.; Roth, S.; *et al*. Raman Spectrum of Graphene and Graphene Layers. *Phys. Rev. Lett.* **2006,** *97,* 187401/ 1–187401/4.

18. Graf, D.; Molitor, F.; Ensslin, K.; Stampfer, C.; Jungen, A.; Hierold, C.; Wirtz, L. Spatially Resolved Raman Spectroscopy of Single- and Few-Layer Graphene. *Nano Lett.* **2007,** *7,* 238–242.

19. Gupta, A.; Chen, G.; Joshi, P.; Tadigadapa, S.; Eklund, P. C. Raman Scattering from High-Frequency Phonons in Supported N-Graphene Layer Films. *Nano Lett.* **2006,** *6,* 2667–2673.

20. Liu, L.; Ryu, S.; Tomasik, M. R.; Stolyarova, E.; Jung, N.; Hybertsen, M. S.; Steigerwald, M. L.; Brus, L. E.; Flynn, G. W. Graphene Oxidation: Thickness Dependent Etching and Strong Chemical Doping. *Nano Lett.* **2008,** *8,* 1965.

21. Ryu, S.; Han, M. Y.; Maultzsch, J.; Heinz, T. F.; Kim, P.; Steigerwald, M. L.; Brus, L. E. Reversible Basal Plane Hydrogenation of Graphene. *Nano Lett.* **2008,** *8,* 4597–4602.

22. Liu, H.; Ryu, S.; Chen, Z.; Steigerwald, M. L.; Nuckolls, C.; Brus, L. E. Photochemical Reactivity of Graphene. *J. Am. Chem. Soc.* **2009,** *131,* 17099–17101.

23. Ferrari, A. C.; Robertson, J. Interpretation of Raman Spectra of Disordered and Amorphous Carbon. *Phys. Rev. B* **2000,** *61,* 14095–14107.

24. Yan, J.; Zhang, Y.; Kim, P.; Pinczuk, A. Electric Field Effect Tuning of Electron-Phonon Coupling in Graphene. *Phys. Rev. Lett.* **2007,** *98,* 166802/1–166802/4.

25. Pisana, S.; Lazzeri, M.; Casiraghi, C.; Novoselov, K. S.; Geim, A. K.; Ferrari, A. C.; Mauri, F. Breakdown of the Adiabatic Born-Oppenheimer Approximation in Graphene. *Nat. Mater.* **2007,** *6,* 198–201.

26. Hod, O.; Barone, V.; Peralta, J. E.; Scuseria, G. E. Enhanced Half-Metallicity in Edge-Oxidized Zigzag Graphene Nanoribbons. *Nano Lett.* **2007,** *7,* 2295–2299.

27. Yan, Q. M.; Huang, B.; Yu, J.; Zheng, F. W.; Zang, J.; Wu, J.; Gu, B. L.; Liu, F.; Duan, W. H. Intrinsic Current-Voltage Characteristics of Graphene Nanoribbon Transistors and Effect of Edge Doping. *Nano Lett.* **2007,** *7,* 1469–1473.

28. Gillen, R.; Mohr, M.; Thomsen, C.; Maultzsch, J. Vibrational Properties of Graphene Nanoribbons by First-Principles Calculations. *Phys. Rev. B* **2009,** *80,* 155418.

29. Kudin, K. N. Zigzag Graphene Nanoribbons with Saturated Edges. *Acs Nano* **2008,** *2,* 516–522.

30. Zhou, J.; Dong, J. Vibrational Property and Raman Spectrum of Carbon Nanoribbon. *Appl. Phys. Lett.* **2007,** *91,* 173108.

31. Gillen, R.; Mohr, M.; Maultzsch, J. Symmetry Properties of Vibrational Modes in Graphene Nanoribbons. *Phys. Rev. B* **2010,** *81,* 205426.

32. Hornekaer, L.; Rauls, E.; Xu, W.; Sljivancanin, Z.; Otero, R.; Stensgaard, I.; Laegsgaard, E.; Hammer, B.; Besenbacher, F. Clustering of Chemisorbed H(D) Atoms on the Graphite (0001) Surface Due to Preferential Sticking. *Phys. Rev. Lett.* **2006,** *97,* 186102.

33. Tuinstra, F.; Koenig, J. L. Raman Spectrum of Graphite. *J. Chem. Phys.* **1970,** *53,* 1126.

34. Cançado, L. G.; Takai, K.; Enoki, T.; Endo, M.; Kim, Y. A.; Mizusaki, H.; Jorio, A.; Coelho, L. N.; Magalhães-Paniago, R.; Pimenta, M. A. General Equation for the Determination of the Crystallite Size La of Nanographite by Raman Spectroscopy. *Appl. Phys. Lett.* **2006,** *88,* 163106.

35. Ferrari, A. C. Raman Spectroscopy of Graphene and Graphite: Disorder, Electron-Phonon Coupling, Doping and Nonadiabatic Effects. *Solid State Commun.* **2007,** *143,* 47–57.

36. Wang, X. R.; Ouyang, Y. J.; Li, X. L.; Wang, H. L.; Guo, J.; Dai, H. J. Room-Temperature All-Semiconducting Sub-10-nm Graphene Nanoribbon Field-Effect Transistors. *Phys. Rev. Lett.* **2008,** *100,* 206803.

37. Casiraghi, C.; Hartschuh, A.; Qian, H.; Piscanec, S.; Georgi, C.; Fasoli, A.; Novoselov, K. S.; Basko, D. M.; Ferrari, A. C. Raman Spectroscopy of Graphene Edges. *Nano Lett.* **2009,** *9,* 1433–1441.

38. Lucchese, M. M.; Stavale, F.; Ferreira, E. H. M.; Vilani, C.; Moutinho, M. V. O.; Capaz, R. B.; Achete, C. A.; Jorio, A. Quantifying Ion-Induced Defects and Raman Relaxation Length in Graphene. *Carbon* **2010,** *48,* 1592–1597.

39. Basko, D. M. Theory of Resonant Multiphonon Raman Scattering in Graphene. *Phys. Rev. B* **2008,** *78,* 125418.

40. Cancado, L. G.; Pimenta, M. A.; Neves, B. R. A.; Dantas, M. S. S.; Jorio, A. Influence of the Atomic Structure on the Raman Spectra of Graphite Edges. *Phys. Rev. Lett.* **2004,** *93,* 247401.

41. Berger, C.; Song, Z. M.; Li, X. B.; Wu, X. S.; Brown, N.; Naud, C.; Mayou, D.; Li, T. B.; Hass, J.; Marchenkov, A. N.; *et al.* Electronic Confinement and Coherence in Patterned Epitaxial Graphene. *Science* **2006,** *312,* 1191–1196.

42. Cancado, L. G.; Pimenta, M. A.; Neves, B. R. A.; Medeiros-Ribeiro, G.; Enoki, T.; Kobayashi, Y.; Takai, K.; Fukui, K.; Dresselhaus, M. S.; Saito, R.; *et al.* Anisotropy of the Raman Spectra of Nanographite Ribbons. *Phys. Rev. Lett.* **2004,** *93,* 047403.

43. Ryu, S.; Liu, L.; Berciaud, S.; Yu, Y.-J.; Liu, H.; Kim, P.; Flynn, G. W.; Brus, L. E. Atmospheric Oxygen Binding and Hole Doping in Deformed Graphene on a SiO$_2$ Substrate. *Nano Lett.* **2010,** *10,* 4944–4951.

44. Paredes, J. I.; Martinez-Alonso, A.; Tascon, J. M. D. Multiscale Imaging and Tip-Scratch Studies Reveal Insight into the Plasma Oxidation of Graphite. *Langmuir* **2007,** *23,* 8932–8943.

45. Leenaerts, O.; Partoens, B.; Peeters, F. M. Adsorption of H$_2$O, NH$_3$, CO, NO$_2$, and NO on Graphene: A First-Principles Study. *Phys. Rev. B* **2008,** *77,* 125416.

46. Dukovic, G.; White, B.; Zhou, Z.; Wang, F.; Jockusch, S.; Heinz, T.; Turro, N.; Friesner, R.; Brus, L. Reversible Surface Oxidation and Efficient Luminescence Quenching in Semiconductor Single-Wall Carbon Nanotubes. *J. Am. Chem. Soc.* **2004,** *126,* 15269.

47. Abdula, D.; Ozel, T.; Kang, K.; Cahill, D. G.; Shim, M. Environment-Induced Effects on the Temperature Dependence of Raman Spectra of Single-Layer Graphene. *J. Phys. Chem. C* **2008,** *112,* 20131–20134.

48. Malard, L. M.; Moreira, R. L.; Elias, D. C.; Plentz, F.; Alves, E. S.; Pimenta, M. A. Thermal Enhancement of Chemical Doping in Graphene: A Raman Spectroscopy Study. *J. Phys.: Condens. Matter* **2010,** *22,* 334202.

49. Nourbakhsh, A.; Cantoro, M.; Klekachev, A.; Clemente, F.; Soree, B.; van der Veen, M. H.; Vosch, T.; Stesmans, A.; Sels, B.; De Gendt, S. Tuning the Fermi Level of SiO$_2$-Supported Single-Layer Graphene by Thermal Annealing. *J. Phys. Chem. C* **2010,** *114,* 6894–6900.

50. Ni, Z. H.; Wang, H. M.; Luo, Z. Q.; Wang, Y. Y.; Yu, T.; Wu, Y. H.; Shen, Z. X. The Effect of Vacuum Annealing on Graphene. *J. Raman Spectrosc.* **2010,** *41,* 479–483.

51. Das, A.; Pisana, S.; Chakraborty, B.; Piscanec, S.; Saha, S. K.; Waghmare, U. V.; Novoselov, K. S.; Krishnamurhthy, H. R.; Geim, A. K.; Ferrari, A. C.; *et al.* Monitoring Dopants by Raman Scattering in an Electrochemically Top-Gated Graphene Transistor. *Nat. Nanotechnol.* **2008,** *3,* 210–215.

52. Bao, W.; Miao, F.; Chen, Z.; Zhang, H.; Jang, W.; Dames, C.; Lau, C. N. Controlled Ripple Texturing of Suspended Graphene and Ultrathin Graphite Membranes. *Nat. Nanotechnol.* **2009,** *4,* 562.

53. Knox, K. R.; Wang, S.; Morgante, A.; Cvetko, D.; Locatelli, A.; Mentes, T. O.; Niño, M. A.; Kim, P.; R., M. O., Jr. Spectromicroscopy of Single and Multilayer Graphene Supported by a Weakly Interacting Substrate. *Phys. Rev. B* **2008,** *78,* 201408.

54. Sharma, R.; Baik, J. H.; Perera, C. J.; Strano, M. S. Anomalously Large Reactivity of Single Graphene Layers and Edges toward Electron Transfer Chemistries. *Nano Lett.* **2010,** *10,* 398–405.